JOURNAL OF MATERIALS SCIENCE **35** (2000) 3647–3654

An elastic-viscoplastic constitutive model for the hot-forming of aluminum alloys*

S. SANTHANAM
Mechanical Engineering Department, Villanova University, Villanova, PA, USA
E-mail: sridhar.santhanam@villanova.edu

Under hot-forming conditions characterized by high homologous temperatures and strain-rates, metals usually exhibit rate-dependent inelastic behavior. An elastic-viscoplastic constitutive model is presented here to describe metal behavior during hot-forming. The model uses an isotropic internal variable to represent the resistance offered to plastic deformation by the microstructure. Evolution equations are developed for the inelastic strain and the deformation resistance based on experimental results. A methodology is presented for extracting model parameters from constant true strain-rate compression tests performed at different temperatures. Model parameters are determined for an Al-1Mn alloy and an Al-Mg-Si alloy, and the predictions of the model are shown to be in good agreement with the experimental data.

1. Introduction

Metal-Forming operations such as Rolling and Forging are frequently performed at high homologous temperatures (0.6 to 0.9) and high strain rates (10^{-3} to 10^{2} sec^{-1}). The metal is also subjected to large deformations and rotations. Designing appropriate tooling to handle these extreme conditions is obviously challenging. In the past, the design process was guided primarily by experimental trial-and-error and empirical modeling. This process is being supplemented today by numerical simulation of the forming process. Numerical simulations have been made possible by the increased understanding of material behavior as well as the rapid progress in computing power.

An important ingredient in numerical simulation of metal forming is an accurate description of the constitutive behavior of the metal. Due to the high homologous temperatures in hot forming, plastic behavior tends to be strain-rate sensitive i.e. viscoplastic. Viscoplastic constitutive equations are widely used in finite-element modeling of hot-forming [1–6]. The constitutive behavior of a given material is usually determined by uniaxial testing in compression, tension, and/or torsion in the temperature and strain-rate regime of interest. A uniaxial model is first constructed and then incorporated into a multi-dimensional framework such as the Norton-Hoff model [1–3] or the Perzyna model [4, 5]. Traditionally, uniaxial models [6–8] express the flow stress as a function of the process parameters and several constants which are established experimentally. These models are empirical and describe material behavior without making a direct connection to microstructural changes that are the root cause of rate-sensitivity.

A rising trend in thermomechanical constitutive modeling is the use of internal variables [9–13]. These variables are used to describe, in a macroscopic average sense, events associated with the development of the microstructure. They characterize average properties associated with dislocation motion, and their interaction with grain boundaries, precipitates, and dislocation pile-ups. Internal variables evolve with viscoplastic deformation and this evolution can be described by rate equations. Typically these variables are not directly measurable but they can be quantified using external variables such as stress, strain, strain rate, and temperature. A fundamental tenet of internal variable based constitutive modeling is that the inelastic strain rate at any instant is governed by the current values of the external and internal variables. History dependence is included in the model through the evolution of the internal variables.

A number of internal variable models exist and have been used extensively in design applications too. Most though have been developed specifically for creep and small strain plasticity [9–12]. The strains and strain rates of interest in this regime do not exceed 5% and 10^{-2} sec^{-1}, respectively. Strains and strain-rates in hot metal forming are considerably higher. There are fewer internal variable models [13–15] available for these applications. Anand's model [13, 14] uses a single internal variable which characterizes the internal isotropic resistance offered by the microstructure to deformation. Sample *et al.* [15] have formulated constitutive models for the plastic working regime that use two internal state variables. In these models, specific functional forms are chosen for the inelastic strain rate and the evolution rate(s) of the isotropic internal variable(s). The choice of these functions is guided either by experiments or theoretical models governing dislocations and their interaction with barriers.

* This work was done when the author was a Visiting Scientist in the Department of Mechanical Engineering at the Indian Institute of Science, Bangalore.

Here, an internal variable based elastic-viscoplastic constitutive model is presented for two Aluminum alloys, an Al-1Mn alloy (0.38% Fe, 1.01% Mn, 0.016% Mg, 0.14% Si, 0.0184% others, rest Al) and an Al-Mg-Si alloy (1.7% Mg, 0.6% Si, 0.3% Cu, 0.2% Cr, 0.2% Fe, 0.23% Mn, 0.22% others, rest Al). In the next section, functions will be presented for the inelastic strain-rate and the rate of evolution of the internal variable. The reasons for the choices are also detailed in this section. Next, a methodology for estimating the model parameters from a sequence of compression tests is outlined. Finally, model parameters are calculated for the two alloys and the effectiveness of the model is verified by comparing its predictions with the compression test results.

2. Elastic-viscoplastic model

Most internal-variable thermomechanical constitutive models have at least two types of internal variables to describe the evolution of microstructure [16]. The first type is a scalar which attempts to capture isotropic hardening/softening phenomena such as dislocation forests, interaction of dislocations with precipitates, subgrains etc. This scalar will be represented here by the symbol s. The second kind of internal variable is a second order tensorial quantity which resembles a stress-like variable. It is commonly referred to as back-stress and denoted by α_{ij}. It arises due to the interaction of a dislocation with a dislocation pile-up and other barriers.

The model presented here has just one isotropic internal variable, s, and no back stress tensorial variable. This allows the model to be simple, but it limits its validity to only monotonic loading situations where there is no significant texture development. There are a number of metal-forming problems where such a model would be tenable.

A single scalar internal variable model requires two equations; a kinetic equation and a scalar evolution equation. The kinetic equation will have the following general form:

$$\dot{\bar{\epsilon}}^{\mathrm{p}} = \dot{\bar{\epsilon}}^{\mathrm{p}}(\bar{\sigma}, s, T) \tag{1}$$

where $\dot{\bar{\epsilon}}^{\mathrm{p}}$ is the effective nonlinear rate of deformation, $\bar{\sigma}$ is the effective Cauchy stress, s is the isotropic internal variable representing deformation resistance, and T is the temperature. The scalar evolution equation has the form:

$$\dot{s} = \dot{s}(\bar{\sigma}, \dot{\bar{\epsilon}}^{\mathrm{p}}, s, T) \tag{2}$$

where $\dot{s}$ is the time rate of evolution of s. Once suitable forms are selected for the functions on the right hand side, these equations can be incorporated into a three-dimensional constitutive framework as will be shown later.

The following functional form is suggested for the kinetic equation:

$$\dot{\bar{\epsilon}}^{\mathrm{p}} = A \exp\left(\frac{-Q}{RT}\right) \exp\left(\frac{\bar{\sigma}}{s}\right)^{m} \tag{3}$$

The three material parameters in this equation are A, Q, and m. Q, here, is an activation energy, while R is the universal gas constant. The presence of $\exp(\frac{-Q}{RT})$ is motivated by the fact that plastic deformation processes such as dislocation glide and climb are thermally activated [17]. The parameters A and Q are assumed to be temperature independent. The term $\exp(\frac{\bar{\sigma}}{s})^{m}$ embodies both the exponential and power-law form, forms that are commonly used to relate steady state strain-rate to steady state stress [17]. The exponent m is a measure of the strain-rate sensitivity. In Anand's model the kinetic equation is expressed as [14]:

$$\dot{\bar{\epsilon}}^{\mathrm{p}} = A \exp\left(\frac{-Q}{RT}\right) \left[\sinh \frac{\xi \bar{\sigma}}{s}\right]^{\frac{1}{m}} \tag{4}$$

The hyperbolic sine term is a modification of Garofalo's sinh function [18] to model steady-state creep. This form is also regularly used to model steady-state hot-forming behavior in metals [6, 19]. Historically, the $\sinh(x)$ function has provided a good empirical fit to steady state data. The exponential form in Equation 3 is preferred here since it is more closely linked to dislocation mechanisms as suggested by Bodner and Partom [17].

The function $\dot{s}(\bar{\sigma}, \dot{\bar{\epsilon}}^{\mathrm{p}}, s, T)$ is next defined. It is assumed to be a linear function of the plastic strain rate $\dot{\bar{\epsilon}}^{\mathrm{p}}$.

$$\dot{s} = f(s, \bar{\sigma}, T)\dot{\bar{\epsilon}}^{\mathrm{p}} \tag{5}$$

This is a very common assumption and has been used in small as well as large strain formulations [16]. The function $f(s, \bar{\sigma}, T)$ should describe dynamic strain hardening as well as dynamic recovery. Static recovery phenomena are more relevant for creep deformation than for hot-forming. They are hence neglected in this model.

When a metal specimen is subjected to a constant true strain rate compression test, a steady state condition is reached wherein $\bar{\sigma}$ approaches a peak steady value. Under these conditions the true strain rate $\dot{\epsilon}$ is nearly equal to the plastic strain rate $\dot{\bar{\epsilon}}^{\mathrm{p}}$ and internal variable s approaches a steady state value too. For such conditions it can be shown, using Equation 3, that:

$$\bar{\sigma} = cs \tag{6}$$

where

$$c = \left[\ln\left\{\left\{\frac{\dot{\bar{\epsilon}}^{\mathrm{p}}}{A}\right\} \exp\left\{\frac{Q}{RT}\right\}\right\}\right]^{\frac{1}{m}} \tag{7}$$

is a constant for a given strain-rate and temperature. Hence the evolution equation for s can be rewritten in terms of $\bar{\sigma}$:

$$\dot{\bar{\sigma}} = cf(s, \bar{\sigma}, T)\dot{\bar{\epsilon}}^{\mathrm{p}} \tag{8}$$

which in turn can be reexpressed as:

$$\frac{\mathrm{d}\bar{\sigma}}{\mathrm{d}\bar{\epsilon}^{\mathrm{p}}} = cf(s, \bar{\sigma}, T) \tag{9}$$

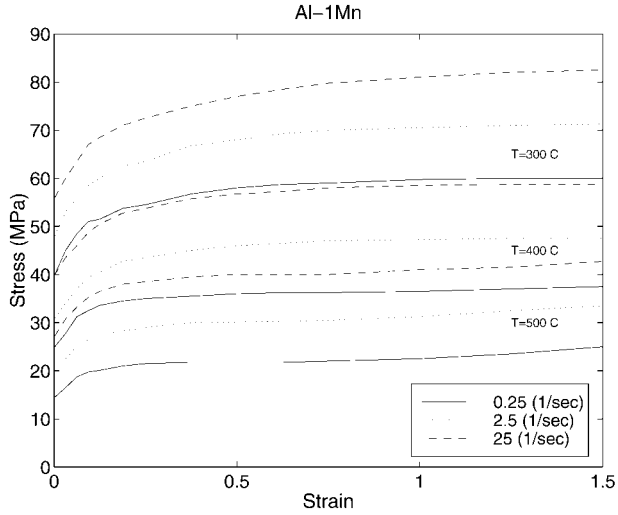

Figure 1 Experimental true stress-strain curves for an Al-1Mn alloy (Shi *et al.* [6]). $T = 300$ C, 400 C, 500 C; strain-rate = 0.25, 2.5, 25 (1/sec.).

In section 4 of this paper, results are presented that pertain to the application of the proposed model to a series of isothermal, constant true strain rate tests performed on an Al-1Mn alloy [6] and an Al-Mg-Si alloy [20]. The data obtained from these tests are presented in Figs 1 and 2 in the form of true-stress versus true-strain graphs for different strain-rates at constant temperatures. Fig. 3 shows $\frac{d\bar{\sigma}}{d\bar{\epsilon}^p}$ as a function of $\bar{\sigma}$ for different strain-rates at $T = 500^\circ$C for the Al-1Mn alloy. Fig. 4 shows the same for the Al-Mg-Si alloy at $T = 450^\circ$C. These figures reveal that there is a steep drop in $\frac{d\bar{\sigma}}{d\bar{\epsilon}^p}$ with increasing $\bar{\sigma}$ followed by a gradual decline to zero as the saturation value of $\bar{\sigma}$ is approached. The following functional form is suggested for $f(\bar{\sigma}, s, T)$ based on Figs 3 and 4:

$$f(\bar{\sigma}, s, T) = f_0 \tan\left(\frac{\alpha\pi}{2}\left(1 - \frac{s}{s^*}\right)\right) \qquad (10)$$

f_0 and α are material constants. s^* is the saturation value of s for a given temperature/strain-rate pair. For s^* an expression identical to that of Anand [13] is adopted:

$$s^* = \tilde{s}\left[\frac{\dot{\bar{\epsilon}}^p}{A}\exp\left(\frac{Q}{RT}\right)\right]^n \qquad (11)$$

$\tilde{s}$ and n are additional material parameters. The use of the tangent function allows the steep drop in Figs 3 and 4 to be captured. Anand chooses to use a power function to model the data of Figs 3 and 4 [13]:

$$f(\bar{\sigma}, s, T) = f_0\left|1 - \frac{s}{s^*}\right|^a \operatorname{sign}\left(1 - \frac{s}{s^*}\right) \qquad (12)$$

Here, $|x|$ and sign(x) denote the absolute value and the sign of x, respectively. The absolute value and the sign functions were introduced by Anand to accommodate situations where the current value of s is greater than the saturation value s^* as can happen when there is a sudden drop in strain-rate or rise in temperature.

In the proposed model, the tangent function of Equation 10 is preferred over the power function of Equation 12 on two counts. Firstly, it is better able to describe the steep drop in Figs 3 and 4. This will be demonstrated in section 4. Secondly, the tangent function naturally takes care of situations where the current value of s exceeds the saturation value s^*.

The principal equations of the proposed model are (3), (5), (10), and (11). These will now be incorporated

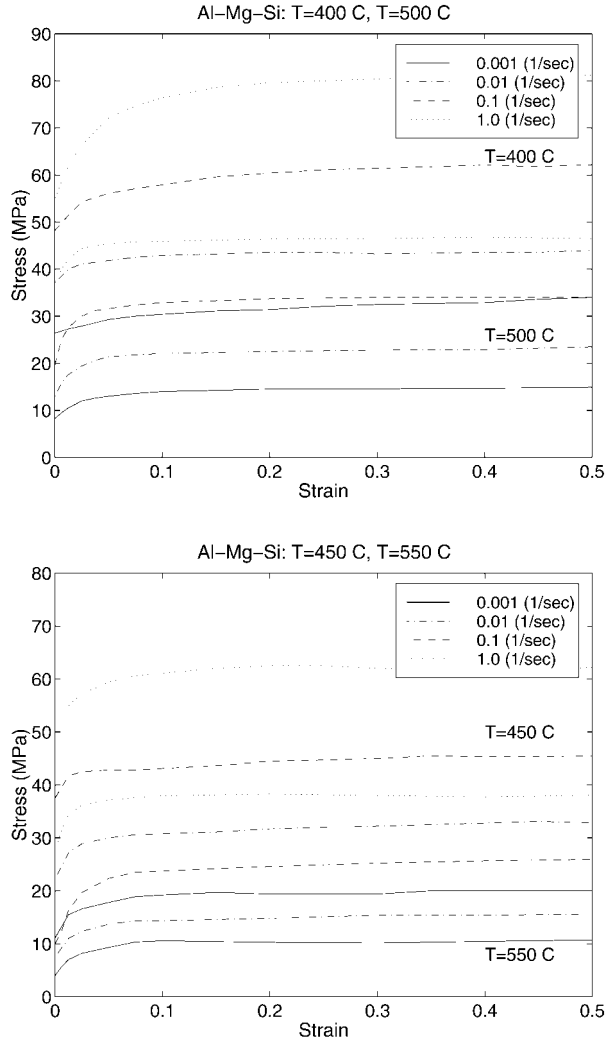

Figure 2 Experimental true stress-strain curves for an as-cast Al-Mg-Si alloy (Sarkar *et al.* [20]). $T = 400$ C, 450 C, 500 C, 550 C; strain-rate = 0.001, 0.01, 0.1, 1.0 (1/sec.).

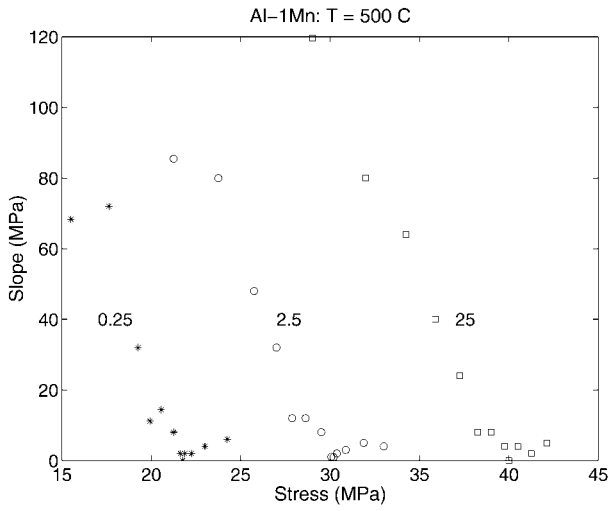

Figure 3 Slope $(\frac{d\bar{\sigma}}{d\bar{\epsilon}^p})$ of experimental true stress-strain curve for Al-1Mn as a function of true stress $(\bar{\sigma})$; $T = 500$ C; strain rate = 0.25, 2.5, 25 (1/sec.).

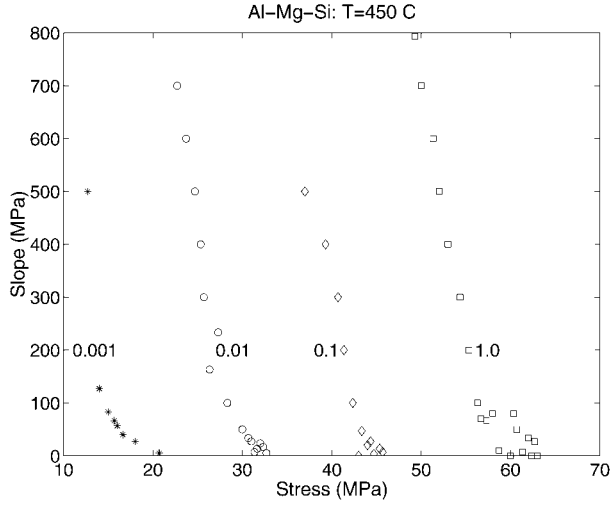

Figure 4 Slope ($\frac{d\bar{\sigma}}{d\bar{\epsilon}^p}$) of experimental true stress-strain curve for Al-Mg-Si alloy as a function of true stress ($\bar{\sigma}$); $T = 450$ C; strain rate = 0.001, 0.01, 0.1, 1.0 (1/sec.).

into a three-dimensional, large deformation constitutive framework. The Cauchy stress tensor σ evolves as:

$$\overset{\circ}{\sigma} = E : [D - D^p] \tag{13}$$

where $\overset{\circ}{\sigma}$ is any one of several possible objective stress rates such as the Jaumann stress rate, E is the fourth-order isotropic elasticity tensor, D is the rate-of-deformation tensor, and D^p is the inelastic part of D. The flow rule for D^p is:

$$D^p = \frac{3\dot{\bar{\epsilon}}^p}{2\bar{\sigma}} S \tag{14}$$

where S is the deviatoric Cauchy stress tensor, $\dot{\bar{\epsilon}}^p$ is the equivalent plastic strain rate as defined by Equation 3, and $\bar{\sigma}$ is the effective von Mises stress. Since $\dot{\bar{\epsilon}}^p$ depends on s, an additional equation for the evolution of s is needed and this is provided by Equations 5 and 10. Equations 13, and 14, coupled with (3), (5), and (10), provide an isothermal constitutive framework. For non-isothermal conditions, an additional energy balance equation will be required to define the evolution of temperature T.

In the next section, a methodology for estimation of model parameters A, Q, m, n, α, $\tilde{s}$, and f_0, is presented.

3. Methodology for parameter estimation

It has been shown that when plastic flow has fully developed, the slope $\frac{d\bar{\sigma}}{d\bar{\epsilon}^p}$ is given by Equation 9. The integrated form of this equation is:

$$\sigma = \sigma^* \left[1 - \frac{2}{\alpha\pi} \arcsin\left(\exp\left\{ \frac{-cf_0 \epsilon^p \alpha\pi}{2\sigma^*} \right\} \times \sin\left\{ \frac{\alpha\pi}{2}\left(1 - \frac{\sigma_0}{\sigma^*}\right)\right\}\right)\right] \tag{15}$$

Here σ and ϵ^p correspond to the true stress and true inelastic strain in a compression test. σ_0 is cs_0 where s_0 is the initial value of the deformation resistance s for a given temperature, and σ^* is the saturation value of compressive stress σ for a given temperature/strain-rate pair.

Another useful equation for parameter estimation is obtained by manipulating Equation 3, once again for the case of fully developed plastic flow. Close to saturation, $\sigma \approx \sigma^*$, $s \approx s^*$, and $\dot{\epsilon} \approx \dot{\epsilon}^p$. Whence,

$$\frac{\dot{\epsilon}}{A} \exp\left\{\frac{Q}{RT}\right\} = \exp\left\{\left(\frac{\sigma^*}{s^*}\right)^m\right\} \tag{16}$$

which leads to

$$\sigma^* = \tilde{s}\left\{\frac{\dot{\bar{\epsilon}}^p}{A}\exp\left(\frac{Q}{RT}\right)\right\}^n \left\{\ln\left(\frac{\dot{\bar{\epsilon}}^p}{A}\exp\left(\frac{Q}{RT}\right)\right)\right\}^{\frac{1}{m}} \tag{17}$$

where Equation 11 has been used for s^*.

Equations 15 and 17 are sufficient to formulate a methodology for determination of A, Q, m, n, α, $\tilde{s}$, and f_0. The procedure for parameter estimation from uniaxial compression test data over the range of strain-rates and temperatures of interest is outlined below.

- The saturation stress σ^* is determined for each strain-rate/temperature pair from Fig. 1 for Al-1Mn and Fig. 2 for Al-Mg-Si.
- For each test, a nonlinear least-squares fit is performed using the functional form of Equation 15. The fit is done directly on the σ vs ϵ^p data. The parameters determined in the process are α, cf_0, and σ_0. While cf_0 and σ_0 are expected to vary from test to test, α should have the same value for all tests. However, there is bound to be some variation and α is therefore determined as the average of the values determined from all tests. Once an adequate estimate of α is obtained the process of nonlinear least-squares fitting is repeated to obtain final values for cf_0 and σ_0 for each test.
- Parameters A, Q, m, n, and $\tilde{s}$ are next found by a nonlinear least-squares fit on Equation 17 using the saturation stress (σ^*) data as a function of strain-rate and temperature.
- Quantity c_i is calculated for each test ($i = 1..N$) using Equation 7. f_0 is then found by averaging:

$$f_0 = \frac{\sum_{i=1}^{N} \frac{(cf_0)_i}{c_i}}{N} \tag{18}$$

where N is the number of tests.
- Equation 15 is revisited and the nonlinear fit process is repeated using the data of Fig. 1 for the parameter σ_0 alone.
- Finally, values for s_0 (initial value of the deformation resistance) are computed by dividing σ_0 by the appropriate value of c for each test. Average values for s_0 are calculated for each temperature by averaging across strain-rates.

4. Model parameters for Al-1Mn and Al-Mg-Si

The data that formed the basis for the parameter estimation for the Al-1Mn alloy were obtained from Shi *et al.* [6] and for the Al-Mg-Si alloy from Sarkar *et al.* [20]. Shi *et al.* [6] performed plane-strain compression tests at equivalent strain rates of 0.25, 2.5, and 25 $\sec^{-1}$. Specimens were prepared from slabs that were chill-cast, homogenized, hot-rolled, and finally heat-treated to get a fully recrystallized structure. Specimens of 10 mm thickness, 50 or 30 mm width, and 60 mm length were then lubricated and deformed to an equivalent strain of 2.0. Sarkar *et al.* [20] performed uniaxial compression tests at four strain-rates (0.001, 0.01, 0.1, 1.0 $\sec^{-1}$) and six temperatures (300, 350, 400, 450, 500, 550°C). The Al-Mg-Si alloy selected had an as-cast dendritic microstructure prior to testing. Specimens of diameter 10 mm and height 15 mm were compressed to half their height. A thermocouple positioned suitably allowed measurement of specimen temperature during the test. Lubrication prevented barreling effects. Each one of the curves in Figs 1 and 2 reveals steady-state or near steady-state behavior. This steady state behavior is a consequence of the balance between work-hardening processes and work softening mechanisms (usually dynamic recovery for aluminum alloys).

Model parameters are obtained based on the procedure outlined in section 3. The nonlinear least-squares fits are performed using subroutines from Numerical Recipes [21]. These routines use the Levenberg-Marquardt method. The estimated values of the parameters for Al-1Mn are listed in Table I and for Al-Mg-Si in Table II. The initial values of the deformation resistance s_0 for Al-1Mn are in Table III and for Al-Mg-Si in Table IV. These numbers by themselves do not validate the model. What is interesting though is that the value of the activation energy Q is 155 kJ/mole for Al-1Mn and 184 kJ/mole for Al-Mg-Si. These numbers are not very different from the activation energy for hot working of typical Aluminum alloys [7]. This activation energy would be expected to correspond to that of the dynamic softening process i.e. dynamic recovery. Dynamic recovery rates are usually dictated by vacancy diffusion. The activation energy for self-diffusion in pure Aluminum is 153 kJ/mole [7]. Our calculated value of 184 kJ/mole for the Al-Mg-Si alloy is somewhat higher but the value of 155 kJ/mole for Al-1Mn is only marginally different.

A possible assessment of the model and its parameters is to numerically simulate the isothermal, constant strain-rate compression tests. In other words, the model should replicate the experimental data from which its parameters have been extracted. This numerical simulation requires a time integration of a set of simultaneous ordinary-differential-equations including Equations 3 and 5 and the following kinematic equation:

$$\dot{\bar{\epsilon}} = \frac{\dot{\bar{\sigma}}}{E} + \dot{\bar{\epsilon}}^{\mathrm{p}} \tag{19}$$

where E is the temperature dependent elastic modulus. These equations are solved by setting $\dot{\bar{\epsilon}}$ equal to the constant strain-rate of the test being simulated. The initial values of $\bar{\sigma}$ and $\bar{\epsilon}^{\mathrm{p}}$ are set to zero while that of s to the value of s_0 at the test temperature. These equations are stiff in nature and therefore need a specialized numerical integration procedure. The 'stiff' subroutine in Numerical Recipes [21] uses an implicit integration procedure and is ideally suited for this task.

The numerical simulations are compared with the experimental stress-strain curves in Figs 5–7 for Al-1Mn and Figs 8–11 for Al-Mg-Si. In almost all cases, the simulated results follow the rise in the experimental stress-strain curves and saturate at the same level of stress. The simulated curves saturate at about the same strain values as the experimental curves do. In isolated instances the simulated saturation-stress is a little different from the actual saturation-stress. For example, in Fig. 11, at a temperature of 550° C and a strain-rate of 1.0 $\sec^{-1}$ for Al-Mg-Si, the simulated saturation stress is 37.0 MPa while the actual saturation stress is 38.0 MPa. The ability of the model to predict saturation

TABLE I Parameters for the elastic-viscoplastic model for Al-1Mn

Model Parameter	Value
A	1.020×10^5 $\sec^{-1}$
Q	155 kJ/mole
m	0.942
n	0.035
$\tilde{s}$	1.24 MPa
f_0	3.99 MPa
α	2.00

TABLE II Parameters for the elastic-viscoplastic model for Al-Mg-Si

Model Parameter	Value
A	1.230×10^5 $\sec^{-1}$
Q	184 kJ/mole
m	0.546
n	0.0289
$\tilde{s}$	0.165 MPa
f_0	0.325 MPa
α	3.85

TABLE III Internal deformation resistance as a function of temperature for Al-1Mn

Temperature (Celsius)	s_0 (MPa)
300	1.80
400	1.57
500	1.32

TABLE IV Internal deformation resistance as a function of temperature for Al-Mg-Si

Temperature (Celsius)	s_0 (MPa)
400	0.221
450	0.206
500	0.181
550	0.175

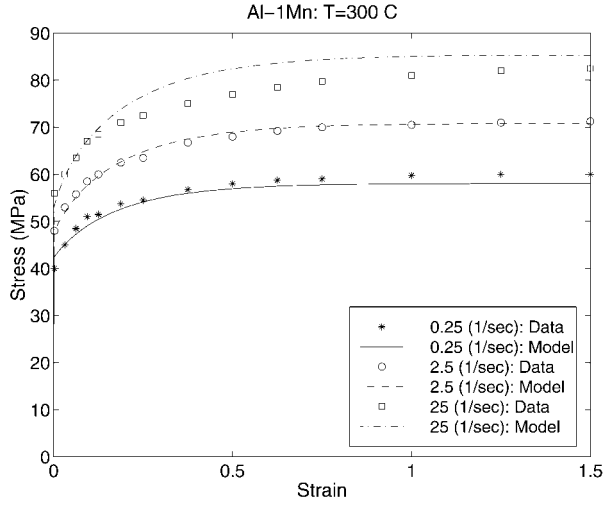

Figure 5 Predicted true stress-strain curve of proposed model (lines) compared with experiment (points) for Al-1Mn; $T = 300$ C; strain rate = 0.25, 2.5, 25 (1/sec.).

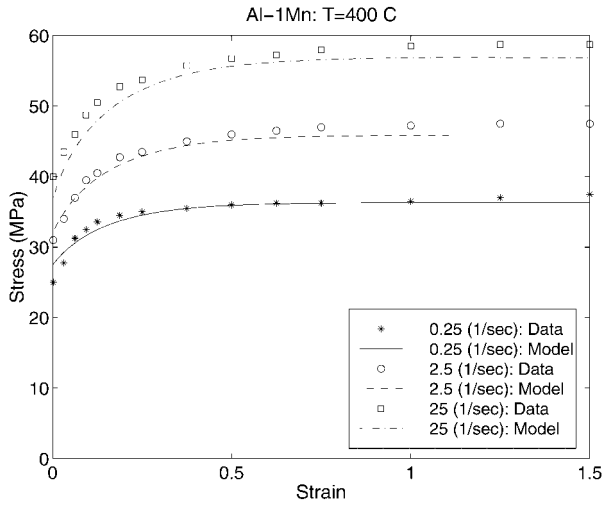

Figure 6 Predicted true stress-strain curve of proposed model (lines) compared with experiment (points) for Al-1Mn; $T = 400$ C; strain rate = 0.25, 2.5, 25 (1/sec.).

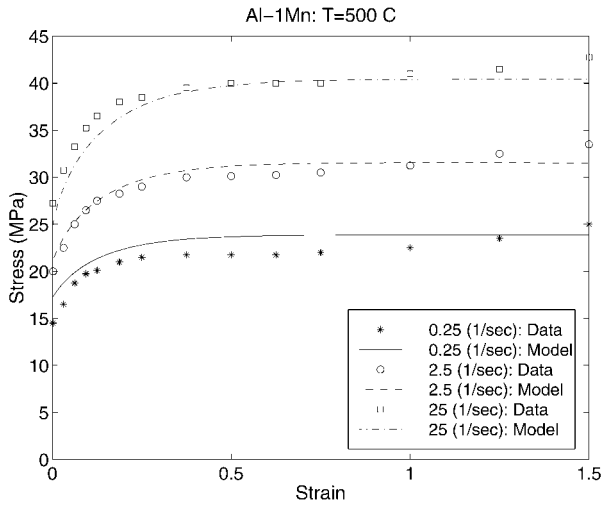

Figure 7 Predicted true stress-strain curve of proposed model (lines) compared with experiment (points) for Al-1Mn; $T = 500$ C; strain rate = 0.25, 2.5, 25 (1/sec.).

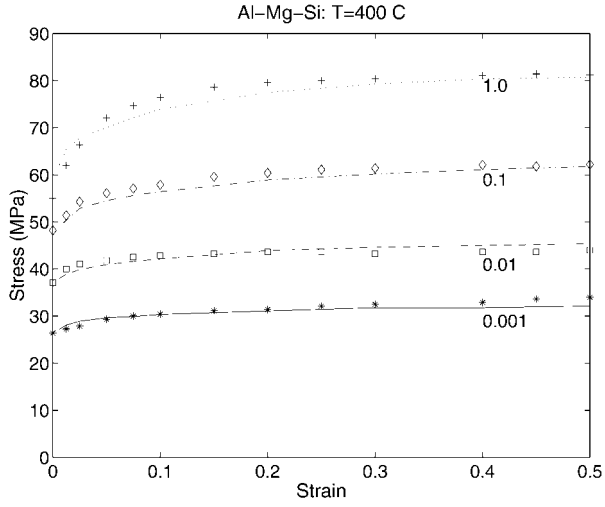

Figure 8 Predicted true stress-strain curve of proposed model (lines) compared with experiment (points) for Al-Mg-Si alloy; $T = 400$ C; strain rate = 0.001, 0.01, 0.1, 1.0 (1/sec.).

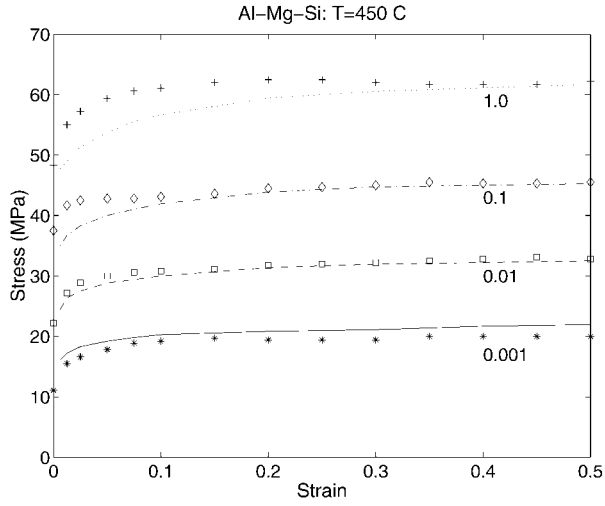

Figure 9 Predicted true stress-strain curve of proposed model (lines) compared with experiment (points) for Al-Mg-Si alloy; $T = 450$ C; strain rate = 0.001, 0.01, 0.10, 1.0 (1/sec.).

stresses at all strain-rates and temperatures is dependent on the Arrhenius factor $\exp\{\frac{Q}{RT}\}$. The use of this term is desirable because it leads to considerable simplification of the model and the process of parameter estimation. But because of its broad generalization it does lead to small errors in prediction of the saturation stresses as is evident from the results of this work as well as others [6, 8]. In any case, instances of a discrepancy between simulated and actual saturation stresses are very few and the error never exceeds 7%.

The simulated curves also follow, to a reasonable extent, the initial steep rise in the experimental curves followed by a rather sharp change in slope as steady state is approached. There are exceptions to this statement as is evident in Figs 9–11 where the simulated curves are unable to follow the experimental curves at a strain-rate of 1.0 sec^{-1}. A possible explanation for this is the existence of more than one hardening/softening mechanism at high temperatures and strain-rates, which would require the use of more than one internal variable. A single internal variable model though is a reasonable

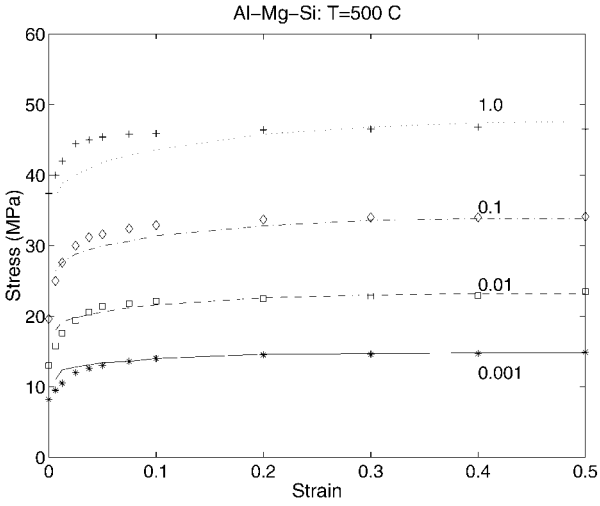

Figure 10 Predicted true stress-strain curve of proposed model (lines) compared with experiment (points) for Al-Mg-Si alloy; $T = 500$ C; strain rate = 0.001, 0.01, 0.1, 1.0 (1/sec.).

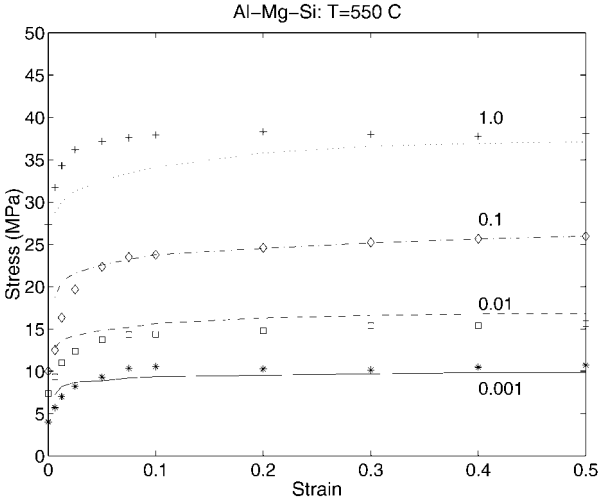

Figure 11 Predicted true stress-strain curve of proposed model (lines) compared with experiment (points) for Al-Mg-Si alloy; $T = 550$ C; strain rate = 0.001, 0.01, 0.1, 1.0 (1/sec.).

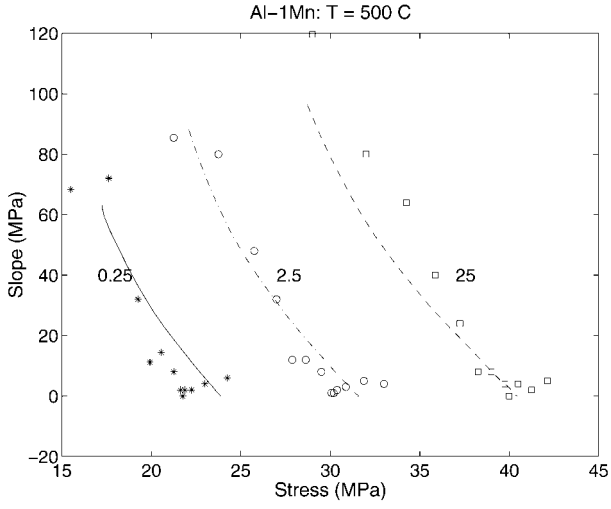

Figure 12 Slope ($\frac{d\bar{\sigma}}{d\bar{\epsilon}^p}$) of true stress-strain curve as a function of true stress ($\bar{\sigma}$): comparison of model prediction (lines) with experiment (points) for Al-1Mn; $T = 500$ C; strain rate = 0.25, 2.5, 25 (1/sec.).

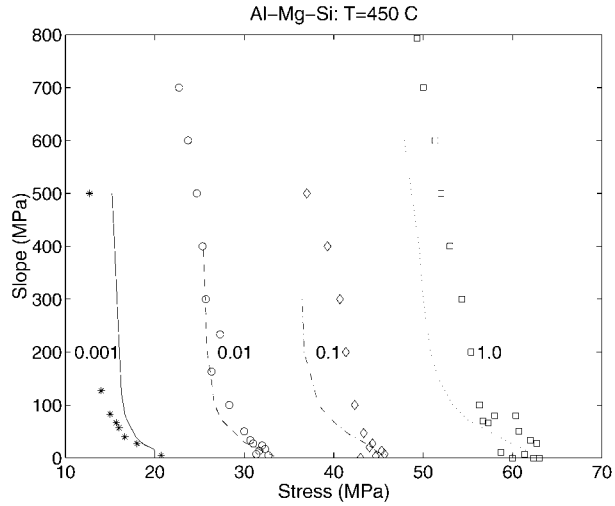

Figure 13 Slope ($\frac{d\bar{\sigma}}{d\bar{\epsilon}^p}$) of true stress-strain curve as a function of true stress ($\bar{\sigma}$): comparison of model prediction (lines) with experiment (points) for Al-Mg-Si alloy; $T = 450$ C; strain rate = 0.001, 0.01, 0.1, 1.0 (1/sec.).

compromise between accuracy and simplicity. Another feature observed in some experimental stress-strain curves is a small droop at large strains. This softening phenomenon is possibly caused by damage accumulation. Our simulations do not predict softening because the model as formulated does not include damage variables. Some strain-strain curves (Fig. 7 for example) actually exhibit a pseudo-hardening after appearing to be saturated. This is primarily due to the failure of the lubricant rather than an intrinsic material behavior.

Figs 12 and 13 present further proof for the ability of the model to recreate the data. These figures compare simulated with experimental $\frac{d\sigma}{d\epsilon^p}$ vs. σ curves for Al-1Mn and Al-Mg-Si at 500°C and 450°C, respectively. Experimental $\frac{d\sigma}{d\epsilon^p}$ were obtained by numerical differentiation of raw σ vs. ϵ^p data. While the simulations do not match the experimental results exactly, the figure does reveal the ability of the tangent function of Equation 10 to describe the steep change in slope.

5. Concluding remarks

Overall the simulated curves resemble the experimental curves in Figs 5 through 11 to a great extent. Hence, the proposed model can be considered as a reasonably accurate description of the hot-forming behavior of the two Aluminum alloys. Additional proof for its validity will depend on its ability to simulate and predict tests that were not used to generate its parameters. Such tests include strain-rate jump tests and constant loading-rate tests. These tests are being conducted and the results will be reported shortly.

A shortcoming of the model is its inability to model softening phenomena. This can be rectified by including damage variables and appropriate damage evolution equations. A second limitation is the fact that the model uses a single scalar internal variable to represent hardening and thus cannot handle extensive texture development. The model parameters have been quantified using uniaxial compression data. In the case of Al-1Mn, compression tests were performed till the specimens

were compressed to 22% of their initial height. For the Al-Mg-Si specimens, compression was performed to 60% of the initial height. Uniaxial compression of face-centered-cubic metals such as aluminum alloys results in a preferred orientation that can be described, rather approximately, as a [110] fiber texture [22]. The orientation density distribution depends on a variety of factors such as strain, strain rate, temperature, alloy composition, and location within the specimen [23]. For the strains, strain rates, temperatures, and alloy compositions under consideration here, the peak value in times random units for the orientation density could range from five to ten (and possibly more) in a (111) pole figure [22, 23]. It would be reasonable to assume that this single scalar variable model can be effectively applied in metal forming problems where the texture development is not significantly different from that of these uniaxial compression specimens.

The elastic-viscoplastic equations presented here are fairly general and should be applicable to materials other than Al-1Mn and Al-Mg-Si. It should be useful for modeling the hot-forming behavior of a large class of metallic alloys in the range of strain-rates from 0.001 to 100.0 sec^{-1}. It should also prove to be an effective constitutive model for incorporation in finite-element simulation of hot-forming processes.

Acknowledgements

The Author wishes to thank Professor Y. V. R. K. Prasad of the Department of Metallurgy, Indian Institute of Science, Bangalore, for the many interesting discussions on high temperature testing of alloys as well as for graciously providing test data on the Al-Mg-Si alloy. The author is also grateful to the Department of Mechanical Engineering, Indian Institute of Science, Bangalore.

References

1. C. BERTRAND-ROSSINI *et al.*, "Modeling of Metal-Forming Processes" (Kluwer Academic Publishers, Dordrecht, The Netherlands, 1988) p. 271.
2. J. M. RIGAUT, D. LOCHEGNIES, J. OUDIN, J. C. GELIN and Y. RAVALARD, "Modeling of Metal-Forming Processes" (Kluwer Academic Publishers, Dordrecht, The Netherlands, 1988) p. 261.
3. C. R. BOER, N. REBELO, H. RYDSTAD and G. SCHRODER, "Process Modeling of Metal-Forming and Thermomechanical Treatment" (Springer-Verlag Berlin, Heidelberg, 1986).
4. D. IDDAN and J. R. TIROSH, *Journal of Applied Mechanics* **63** (1996) 27.
5. O. C. ZIENKIEWICZ and P. N. GODBOLE, *International Journal for Numerical Methods in Engineering* **8** (1974) 3.
6. H. SHI, A. J. MCLAREN, C. M. SELLARS, R. SHAHANI and R. BOLINGBROKE, *Materials Science and Technology* **13** (1997) 210.
7. T. SHEPPARD and A. JACKSON, *ibid.* **13** (1997) 203.
8. J. M. CABRERA, J. J. JONAS and J. M. PRADO, *ibid.* **12** (1996) 579.
9. S. R. BODNER, in "Unified Constitutive Equations for Creep and Plasticity," edited by A. K. Miller (Elsevier Applied Science, New York, 1987) p. 273.
10. A. K. MILLER, in "Unified Constitutive Equations for Creep and Plasticity," edited by A. K. Miller (Elsevier Applied Science, New York, 1987) p. 139.
11. M. A. ROWLEY and E. A. THORNTON, *Journal of Engineering Materials and Technology* **118** (1996) 19.
12. A. F. SKIPOR, S. V. HARREN and J. BOTSIS, *ibid.* **118** (1996) 1.
13. L. ANAND, *ibid.* **104** (1982) 12.
14. S. B. BROWN, K. H. KIM and L. ANAND, *International Journal of Plasticity* **5** (1989) 95.
15. V. M. SAMPLE, L. A. LALLI and O. RICHMOND, "Modeling the Deformation of Crystalline Solids" (TMS, Warrendale, PA, 1991) p. 327.
16. D. C. STOUFFER and L. T. DAME, "Inelastic Deformation of Metals: Models, Mechanical Properties, and Metallurgy" (John Wiley and Sons, New York, 1996).
17. S. R. BODNER and Y. PARTOM, *Journal of Applied Mechanics* **42** (1975) 385.
18. F. GAROFALO, *Transactions AIME* **227** (1963) 351.
19. J. J. JONAS, C. M. SELLARS and W. J. MCG. TEGART, *Metallurgical Reviews* **14** (1969) 1.
20. J. SARKAR, Y. V. R. K. PRASAD and M. K. SURAPPA, *Journal of Materials Science* **30** (1995) 2843.
21. W. H. PRESS, S. A. TEUKOLSKY, W. T. VETTERLING and B. P. FLANNERY, "Numerical Recipes in FORTRAN: The Art of Scientific Computing," 2nd ed. (Cambridge University Press, 1992).
22. C. S. BARRETT and T. B. MASSALSKI, "Structure of Metals," 3rd ed. (McGraw Hill, 1966).
23. Z. JIN, G. T. GRAY and Y. W. KIM, *Materials Science and Engineering A* **239** (1997) 729.

Received 18 February 1999
and accepted 3 February 2000